# Important role of matrix metalloproteinase 9 in epileptogenesis

Grzegorz M. Wilczynski,[1,3] Filip A. Konopacki,[1,2,5] Ewa Wilczek,[4] Zofia Lasiecka,[1] Adam Gorlewicz,[1] Piotr Michaluk,[2] Marcin Wawrzyniak,[2] Monika Malinowska,[1] Pawel Okulski,[2] Lukasz R. Kolodziej,[2] Witold Konopka,[2] Kamila Duniec,[2,5] Barbara Mioduszewska,[2] Evgeni Nikolaev,[2] Agnieszka Walczak,[1] Dorota Owczarek,[1] Dariusz C. Gorecki,[6] Werner Zuschratter,[7] Ole Petter Ottersen,[8] and Leszek Kaczmarek[2]

[1]Department of Neurophysiology and [2]Department of Molecular and Cellular Neurobiology, Nencki Institute, 02-093 Warsaw, Poland
[3]Department of Histology and Embryology and [4]Department of Pathology, Medical University of Warsaw, 02-005 Warsaw, Poland
[5]Postgraduate School of Molecular Medicine, 02-093 Warsaw, Poland
[6]Institute of Biomedical and Biomolecular Sciences, University of Portsmouth, PO1 2DT Portsmouth, England, UK
[7]Leibniz Institute for Neurobiology, D-39118 Magdeburg, Germany
[8]Centre for Molecular Biology and Neuroscience, Institute of Basic Medical Sciences, University of Oslo, N-0317 Oslo, Norway

Temporal lobe epilepsy (TLE) is a devastating disease in which aberrant synaptic plasticity plays a major role. We identify matrix metalloproteinase (MMP) 9 as a novel synaptic enzyme and a key pathogenic factor in two animal models of TLE: kainate-evoked epilepsy and pentylenetetrazole (PTZ) kindling–induced epilepsy. Notably, we show that the sensitivity to PTZ epileptogenesis is decreased in MMP-9 knockout mice but is increased in a novel line of transgenic rats overexpressing MMP-9. Immunoelectron microscopy reveals that MMP-9 associates with hippocampal dendritic spines bearing asymmetrical (excitatory) synapses, where both the MMP-9 protein levels and enzymatic activity become strongly increased upon seizures. Further, we find that MMP-9 deficiency diminishes seizure-evoked pruning of dendritic spines and decreases aberrant synaptogenesis after mossy fiber sprouting. The latter observation provides a possible mechanistic basis for the effect of MMP-9 on epileptogenesis. Our work suggests that a synaptic pool of MMP-9 is critical for the sequence of events that underlie the development of seizures in animal models of TLE.

## Introduction

Epilepsy is a chronic neurological disorder affecting 1–3% of mankind. It is defined by recurrent spontaneous seizures that may be generated by synchronous firing of a localized group of neurons, the so-called epileptic foci (Engel, 1996; Pitkanen and Sutula, 2002). Temporal lobe epilepsy (TLE) is the most common type of epilepsy in adults. It is characterized by the presence of epileptic foci located within the hippocampal formation, amygdala, or temporal neocortex. Unfortunately, in as many as 70% of patients, TLE is intractable by pharmacologic treatment and requires brain surgery for seizure control. Accordingly, there is an urgent need to understand the molecular mechanisms of this severe disease. Aberrant synaptic plasticity has been postulated to underlie formation of epileptic foci and, thus, molecules implicated in plasticity offer an interesting clue toward understanding the disease.

Matrix metalloproteinases (MMPs) form a large family of structurally related zinc-dependent secreted or cell membrane–bound proteinases that are considered to be major executors of ECM remodeling throughout the body (Sternlicht and Werb, 2001) and of pivotal importance in cancer invasion and metastasis. In the adult brain, MMPs have repeatedly been implicated in various pathologies, including acute and chronic neurodegeneration (e.g., in ischemia, trauma, and Alzheimer's disease), inflammation, and cancer (for review see Yong, 2005). Recent studies also suggest that MMP-9 plays an important role in synaptic plasticity, learning, and memory (Szklarczyk et al., 2002; Meighan et al., 2006; Nagy et al., 2006; Okulski et al., 2007; Tian et al., 2007). As epileptogenic plasticity involves extensive nervous tissue remodeling (Ben-Ari, 2001), we decided to examine the potential pathogenic role of MMP-9 in two distinct animal

Correspondence to Leszek Kaczmarek: L.Kaczmarek@nencki.gov.pl; or Grzegorz M. Wilczynski: G.Wilczynski@nencki.gov.pl

Abbreviations used in this paper: ANOVA, analysis of variance; DG, dentate gyrus; DIV, day in vitro; GFAP, glial fibrillary acidic protein; ICAM, intercellular adhesion molecule; IR, immunoreactivity; KA, kainic acid; KO, knockout; MMP, matrix metalloproteinase; NMDAR, *N*-methyl D-aspartate acid receptor; PSD, postsynaptic density; PTZ, pentylenetetrazole; TG, transgenic; TLE, temporal lobe epilepsy; tPA, tissue plasminogen activator; WT, wild type.

The online version of this paper contains supplemental material.


The Journal of Cell Biology, Vol. 180, No. 5, March 10, 2008 1021–1035
http://www.jcb.org/cgi/doi/10.1083/jcb.200708213

models of TLE: kainate-evoked epilepsy and pentylenetetrazole (PTZ) kindling–induced epilepsy (for review see Morimoto et al., 2004).

Kainate is a neurotoxic agonist of glutamate receptors that induces severe status epilepticus, leading to neurodegeneration in all hippocampal subfields except for the dentate gyrus (DG; Sperk, 1994). Instead of dying, the granule neurons of the DG undergo a sequence of plastic phenomena, including pruning of dendritic spines (Suzuki et al., 1997) and axonal sprouting that involves ingrowth of mossy fibers (granule cell axons) into their parent dendritic field to make recurrent excitatory connections (Sutula et al., 1998). The sprouting is believed to underlie spontaneous seizures that occur in kainate-treated animals after some latency period (for review see Morimoto et al., 2004). It is of interest to note that kainate strongly up-regulates MMP-9 in the DG (Szklarczyk et al., 2002).

Kindling is a repeated electrical or chemical stimulation of the brain that initially does not induce seizures but eventually leads to lowering of the seizure threshold and, finally, to the occurrence of spontaneous seizures that are the hallmark of epilepsy (for review see Morimoto et al., 2004). Kindling is not associated with overt neurodegeneration, yet it induces excessive sprouting of mossy fibers and synaptogenesis, mainly within the mossy fibers' normal terminal field, i.e., at the CA3 pyramidal cells' dendrites (Chen and Strickland, 1997).

Importantly, mechanisms similar to those operating in kainate- and/or kindling-induced animal epilepsy occur during the course of TLE (albeit in a different time frame), as demonstrated by autopsy studies of human epileptic brains (Proper et al., 2000).

In this paper, using the MMP-9 gene knockout (KO), as well as a novel model of MMP-9 overexpression, we show that MMP-9 plays a major role in epileptogenesis. We further demonstrate that MMP-9 protein and enzymatic activity are up-regulated in hippocampal synapses upon seizures, contributing to remodeling of dendritic spines and aberrant synaptogenesis. Our studies have clinical implications, as they identify MMP-9 as a potential pharmacological target in epilepsy.

## Results

### MMP-9 facilitates chemical kindling–induced epilepsy in vivo

We first asked whether deletion of the MMP-9 gene affects epileptogenesis. To avoid any indirect effects of MMP-9 deficiency that could occur in the kainate model because of the well known role of MMP-9 in neuronal death (Jourquin et al., 2003; for review see Yong, 2005), we decided to investigate a chemical kindling model that, in contrast to the kainate model, does not involve neurodegeneration. In the kindling model, animals are given repeated intraperitoneal injections of a subconvulsive dose of PTZ for several weeks. During the course of the experiment, progressive lowering of seizure threshold occurs and the animals start to exhibit seizure behavior, which is aggravated with time (Fig. 1 A). At the end point of such a kindling procedure, the dose that was subconvulsive at the beginning elicits full-blown generalized tonic-clonic seizures.

When we performed PTZ kindling on MMP-9 KO mice and wild-type (WT) controls, no difference was noted in convulsive behavior upon the first injections (Fig. 1 A). Subsequently, when WT mice started to respond with seizures, many MMP-9 KO animals remained insensitive to PTZ. MMP-9–deficient mice eventually developed seizures that progressively increased in score, but the seizures remained less severe than in WT mice (repeated measures analysis of variance [ANOVA]: $F(1,9) = 9.9$; $P < 0.05$). Finally, there was also a difference in survival rate. Thus three out of five WT and one out of six KO died upon generalized seizures during the last phase of the experiment (sign test; $P < 0.05$; Fig. 1 A).

Having identified a protective effect of MMP-9 gene KO, we then asked whether overexpression of MMP-9 would enhance epileptogenesis. To this end, we generated transgenic (TG) rats with constitutive neuronal MMP-9 overexpression under the control of the synapsin I promoter (MMP-9 TG). This procedure resulted in a markedly increased MMP-9 expression and activity in the brain but not in other organs (Fig. S1, available at http://www.jcb.org/cgi/content/full/jcb.200708213/DC1). When we subjected MMP-9 TG rats to PTZ kindling, we observed an increased susceptibility to epileptogenesis as compared with the WT rats (repeated measures ANOVA: $F(1,13) = 4.9$; $P < 0.05$; Fig. 1 B). Essentially the same results were obtained in another line of MMP-9–overexpressing TG rats that we generated (repeated measures ANOVA: $F(1,15) = 5.7$; $P < 0.05$; not depicted).

### MMP-9 is localized to hippocampal synapses and becomes up-regulated therein upon kainate-evoked seizures

We hypothesized that MMP-9 facilitated the development of seizures through an effect on epilepsy-related synaptic plasticity. As a first step toward the understanding of how MMP-9 exerts its influence on dendritic spines, we investigated its fine structural localization in the dendritic layer of the hippocampal DG in control and kainate-treated rats, using light and electron microscopic immunocytochemistry.

In the control DG, confocal microscopy revealed punctate MMP-9 immunostaining throughout the dendritic (molecular) layer and, to a much lesser extent, throughout the layer of neuronal cell bodies (Fig. 2, A and B). A high-power imaging of the DG dendritic field revealed that the majority (72 ± 7%) of MMP-9–immunoreactive foci strictly colocalized with dendrites (as indicated by their overlap with a dendritic marker, MAP-2; Fig. 2 C). Moreover, by labeling MMP-9 in conjunction with the presynaptic marker synaptophysin (Fig. 2, D–G, circles), the postsynaptic marker *N*-methyl D-aspartate acid receptor (NMDAR) subunit NR1 (Fig. 2, H–J, circles), or the dendritic spine protein drebrin (Fig. S2, available at http://www.jcb.org/cgi/content/full/jcb.200708213/DC1), we found that many of the dendritic MMP-9–positive puncta overlapped with, or were located very close to, synapses. Interestingly, at very high magnification, synaptic MMP-9 immunoreactivity (IR) appeared to colocalize more extensively with NR1 than with synaptophysin, which is consistent with an association with postsynaptic rather than presynaptic domains.

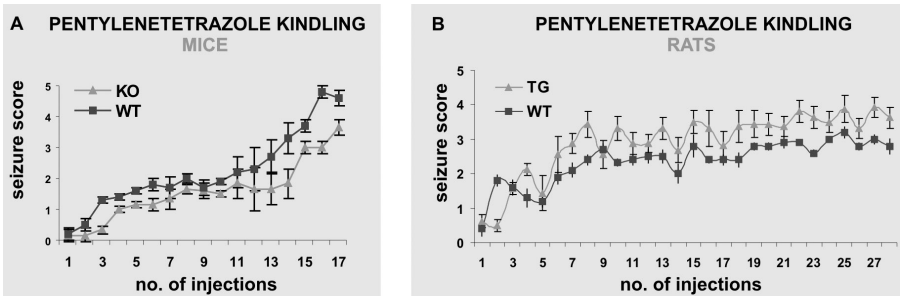


Figure 1. **MMP-9 involvement in PTZ kindling–induced epilepsy.** Seizure scores of PTZ-kindled WT and MMP-9 KO mice (A) and WT and MMP-9–overexpressing TG rats (B) during the course of the experiment. Note that epileptogenesis is delayed in MMP-9 KO mice (repeated measures ANOVA: $F(1,9) = 9.9$; $P < 0.05$). In contrast, epileptogenesis is accelerated in MMP-9–overexpressing TG rats (repeated measures ANOVA: $F(1,13) = 4.9$; $P < 0.05$). Note that the differences in the seizure score between WT and TG animals do not show up upon the first few injections but progressively develop thereafter, thus indicating that a plastic process is involved. Error bars represent SEM.

To explore the subcellular MMP-9 distribution, we used a postembedding immunogold procedure that affords preservation of ultrastructural details as well as protein IR. By this technique, the majority of gold particles were found to be associated with a subset (~50%) of dendritic spine profiles (Fig. 2). Within MMP-9–immunoreactive spines, immunogold particles were present mainly in the spine head, frequently being located adjacent to, or within, postsynaptic densities (PSD) of axospinous (excitatory) synapses (Fig. 2, Q, R, T, and U). Frequently, gold particles were associated with the spine plasma membrane, with some particles being superimposed on the synaptic cleft (Fig. 2, Q, R, and T) and/or extracellular space (Fig. 2, Q and V). Within spines, gold particles were often found in the vicinity of vesicular (Fig. 2, T and V) or tubulovesicular (Fig. 2 U) membrane structures. The quantitative analysis of the labeling density of spine profiles ($7.6 \times 10^{-6}/nm^2$; $n = 92$ spines) confirmed a significant association of gold particles with this compartment, as compared with both background density ($0.4 \times 10^{-6}/nm^2$; $\chi^2 = 77.3$; $P < 0.000001$) and overall gold particle density ($4.4 \times 10^{-6}/nm^2$; $\chi^2 = 26.1$; $P < 0.000001$; see Materials and methods for details) in the section. Interestingly, among spines containing MMP-9 IR, we found a strong negative correlation between the density of gold particles and area of spine profile (Spearman's rank correlation coefficient: $r = 0.72$; $P < 0.05$).

Clusters of gold particles were found not only in spines but also postsynaptic to asymmetrical synapses on dendritic stems (unpublished data). In contrast, the vast majority of axodendritic symmetric (inhibitory) synapses were devoid of gold particles, signaling MMP-9 (Fig. 2 V). We supported this finding using less precise, albeit statistically much more robust, immunofluorescent confocal analysis, showing virtually no colocalization of MMP-9 IR with β2/3 GABA-AR subunits, which mark inhibitory synapses (Fig. 2, K–M). Apart from synaptic sites, MMP-9 IR was also located within vesicular structures in dendritic shafts (Fig. 2 V) and in some small astrocytic processes (not depicted).

Kainate-induced status epilepticus produced profound changes in MMP-9 IR throughout the DG molecular layer that were noticeable over several days after insult. By light microscopy, the punctate MMP-9 IR became strongly increased at 24 h after seizure onset, peaked at 72 h (Fig. 3, A–C), and remained increased at 7 d after insult. Thus, we confirmed our previous results, obtained by immunohistochemistry and Western blotting, showing an increase in MMP-9 IR in the DG after kainate administration (maximum at 72 h; Szklarczyk et al., 2002).

After 24 h, the punctate MMP-9 IR became accompanied by MMP-9 labeling of glial cells (Fig. 3 B). The glial labeling, which derived mainly from astrocytes (based on their IR for glial fibrillary acidic protein [GFAP]; not depicted), increased thereafter, reaching its peak at 7 d after seizure onset (Fig. 3 C).

Quantitative evaluation of MMP-9 and MAP-2 colocalization in the DG molecular layer revealed that the number (per unit area) and fluorescence intensity of the dendrite-associated MMP-9–positive foci increased 5.6 ± 0.1-fold and 6.7 ± 0.2-fold at 24 and 72 h after seizures, respectively (Kruskall-Wallis test; $P < 0.05$). No change was found in the mean area occupied by dendrites, which indicates that these changes could not result from the shrinkage of the tissue. To address the status of MMP-9 IR at the level of synapses, we used preembedding immunoelectron microscopy with silver enhancement of the peroxidase reaction product. No major qualitative changes in the pattern of MMP-9 IR were detected at the ultrastructural level at the 72-h time point, yet the number of MMP-9 IR–containing spine profiles per unit area increased by a factor of 2.2 ± 0.1 (*t* test; $P < 0.05$; Fig. 3 M).

### Synaptodendritic MMP-9 enzymatic activity increases after kainate treatment

After obtaining the immunocytochemical data, it became necessary to determine whether synaptic MMP-9 is active and whether this activity is regulated by seizures. To this end, we performed both in situ and gel zymography of subcellular fractions to compare control brains and brains of kainate-injected animals 24 h after the onset of seizures. We showed previously that kainate-induced up-regulation of the bulk gelatinolytic activity peaks at this time point (Szklarczyk et al., 2002).

To visualize gelatinolytic activity, we established a protocol in which 150-μm thick acutely isolated hippocampal slices were incubated with a fluorogenic substrate (DQ gelatin) in the tissue culture incubator. The experiments demonstrated gelatinase activity to be present in the cell bodies of granule neurons (not depicted) and in the neuropil of the molecular layer (Fig. 4, A, C, D, and F). In the latter, there were numerous discrete submicrometer foci of enzymatic activity. Double labeling with anti–MAP-2 antibody revealed that the majority of those foci colocalized with dendrites (Fig. 4, C and F, arrows). Kainate caused

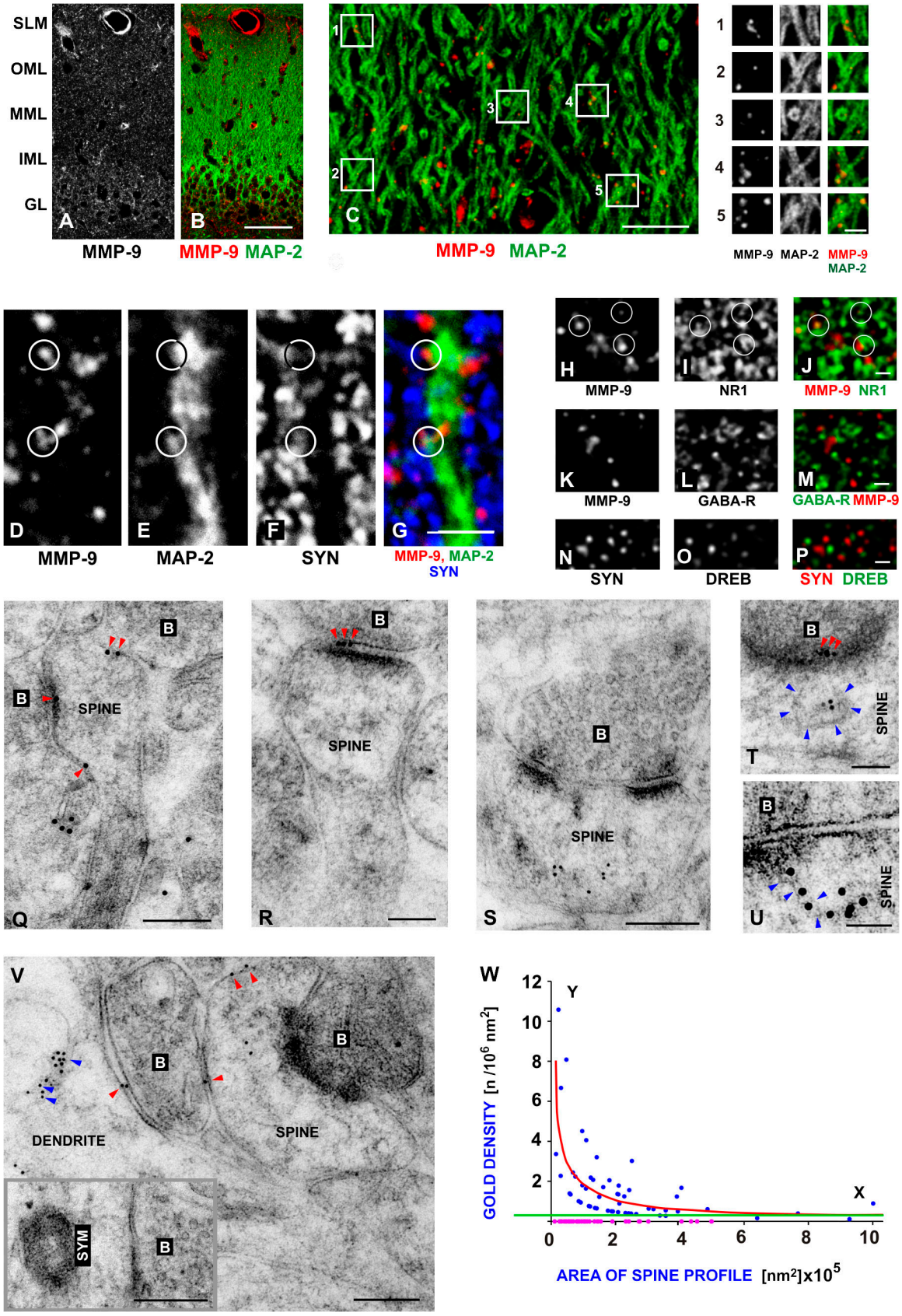


Figure 2. **MMP-9 IR in the control DG.** (A and B) Low-power single-plane confocal images of MMP-9 IR (A) and MMP-9 IR plus MAP-2 IR (B, red and green, respectively) showing predominantly punctate MMP-9 IR in the DG molecular layer. Strong MMP-9 IR is also present within the walls of blood vessels in the stratum lacunosum moleculare (SLM). The anatomical subdivisions of the DG are marked as follows: IML, inner molecular layer; MML, middle molecular layer; OML, outer molecular layer; GL, granular layer. Bar, 75 µm. (C) High-power confocal image of the DG middle molecular layer double stained for

a dramatic increase in the number of dendritic gelatinase spots (Fig. 4, compare C and F).

Gel zymography of subcellular fractions from control hippocampi revealed substantial MMP-9 and MMP-2 activities in total homogenate, but no gelatinase activity was found in the synaptodendrosomal fraction of this sample (Fig. 4 G). Kainate treatment caused an up-regulation of MMP-9, but not MMP-2, in total homogenate and the emergence of a single band of an apparently latent form of MMP-9, but not MMP-2, activity in synaptodendrosomes. Lack of activated MMP-9 (of smaller molecular weight) appears surprising; however, it may result from a washout of the active secreted protein during the biochemical procedure. It is unlikely that 24 h after the kainate treatment only pro–MMP-9 is present at the synapses because the activity clearly shows up in in situ zymography without the SDS treatment that activates the latent MMP-9. However, it should also be noted that a latent form of MMP-9 has been suggested to have some gelatinolytic activity in vivo (Bannikov et al., 2002).

### Seizure-induced dendritic spine pruning involves MMP-9

To investigate whether MMP-9 is functionally involved in seizure-induced spine pruning, we decided to compare the degree of acute spine loss in kainate-treated MMP-9 WT and KO mice. Because MMP-9 KO mice are resistant to the excitotoxic effect of intraperitoneally administered kainate (unpublished data), probably because of their C57BL/6 genetic background (McKhann et al., 2003), we made unilateral kainate injections into the amygdala (according to Wu et al. [2000]) that did result in status epilepticus, followed by characteristic hippocampal CA1-CA3 and hilar degeneration on the injected, but not contralateral, side.

We analyzed in this model the effect of kainate on the spine density in the DG molecular layer of MMP-9 WT and KO mice using Golgi silver impregnation. In WT animals, we found that at 24 h after the onset of seizures, a substantial decrease in the density of spines occurred at the injected side as compared with the contralateral side (Fig. 5 U). In striking contrast, there was no statistically significant difference between the injected and contralateral side in MMP-9 KO mice (Fig. 5 U). Importantly, there were no apparent differences between WT and KO animals in regard to the intensity of seizures. Thus, it appears that MMP-9 KO renders dendritic spines significantly more resistant to kainate-evoked pruning (Fig. 5). Essentially the same results were obtained with another spine marker, fluorophore-conjugated phalloidin (F-actin–specific probe), used in conjunction with the PSD marker ProSAP/Shank (Fig. 5, G–O). Again, in MMP-9–deficient mice, the phalloidin staining of spines was significantly less affected than in WT mice. The spine counts in untreated WT and KO mice did not differ from each other.

### MMP-9 activity is involved in aberrant synaptogenesis after mossy fiber sprouting

Epileptogenesis in the kainate-treated hippocampus begins within ~1 wk after the insult when sprouting mossy fibers start to make recurrent synapses with granule cell dendrites (Suzuki et al., 1997; Sutula et al., 1998; Ben-Ari, 2001). To test whether MMP-9 activity may play a role in aberrant synaptogenesis, we first used rat organotypic hippocampal slices subjected either to kainate excitotoxicity or picrotoxin stimulation and treated with a specific MMP-9 inhibitor.

Organotypic hippocampal cultures retain the typical anatomical features of the hippocampal formation, thus providing an excellent model to study the effects of various molecules on hippocampal structure and function (Jourquin et al., 2003). We treated such cultures with either kainate or vehicle solution. The cultures were then allowed to recover for 2 wk, after which they were fixed and immunostained for synaptoporin, a marker of mossy fiber boutons. Additionally, the cultures were costained for MAP2 to visualize dendrites. This procedure helped also to delineate anatomical subdivisions (Fig. S1). In control cultures, there was an intense synaptoporin IR of the mossy fiber pathway (extending from the dentate hilus up to the end of the CA3 area) but little or no synaptoporin labeling in the DG granular and inner molecular layers (Fig. 6 A and Fig. S1). Kainate treatment at DIV (day in vitro) 9 caused an extensive neurodegeneration (indicated by the loss of MAP2 staining) with a pattern similar to that found in vivo (CA affected, DG spared). The damage was fully developed by 24 h. Importantly, when such cultures were examined at 21 DIV, a dense meshwork of strongly synaptoporin-positive terminals appeared among the granule cells bodies and in their dendritic field, which is indicative of robust mossy fibers sprouting (Fig. 6, B and H; and Fig. S1).

MMP-9 (red) and MAP-2 (green). Bar, 1 μm. (insets 1–5) The majority of MMP-9–immunoreactive puncta strictly colocalize with dendrites. Bar, 5 μm. (D–G) High-power triple immunolabeling for MMP-9 (D; and G, red), MAP-2 (E; and G, green), and synaptophysin (F; and G, blue; paraffin section). Note that dendrite-associated MMP-9–immunoreactive foci frequently lie adjacent to synaptophysin puncta, which represent presynaptic terminals. Circles indicate the sites of triple colocalization, i.e., putative MMP-9–immunoreactive synapses. SYN, synaptophysin. Bar, 2 μm. (H–M) High-power double immunolabeling for MMP-9 (H; J, red; K; and M, red) and either NR1 (I; and J, green) or GABA-R subunits β2/3 (L; and M, green; paraffin sections). Although some of the MMP-9–immunoreactive spots colocalize with NR1 (H–J, circles), virtually none of them colocalize with GABA-R. Bars, 1 μm. (N–P) Control specimen double immunolabeled for synaptophysin (N; and P, red) and the postsynaptic marker drebrin (O; and P, green), the proteins which are known not to colocalize. DREB, drebrin. Bar, 1 μm. (Q–V) Electron microscopic immunogold detection (after embedding) of MMP-9 in the DG molecular layer. The following ultrastructural landmarks are shown: SPINE, dendritic spine; B, presynaptic bouton; and SYM, symmetric synapse. Immunogold particles indicating MMP-9 IR are present at dendritic spines (Q–V) and thin shafts (V), where they associate with the plasma membrane (red arrowheads), including the postsynaptic membrane of asymmetrical (excitatory) synapses (R and T, red arrowheads), and with the cytoplasmic vesicular or tubulovesicular structures (T–V, blue arrowheads). Note the immunonegative symmetric (inhibitory) dendritic shaft synapse (V, inset, SYM). Bars: (R and T) 100 nm; (Q,S,V, and inset) 200 nm; (U) 50 nm. (W) A scatterplot demonstrating the relationship between the size of dendritic spine profile (area of cross section; x axis) and the concentration of MMP-9 IR it contains (approximated by the ratio between the number of gold particles found within the spine cross section and the area of this cross section; y axis). Each spine profile is represented by dots. Blue dots, synapses that contained at least one gold particle; purple dots, immunonegative spine profiles. Curve fitting reveals the essentially exponential form of the relationship among immunoreactive profiles (red line). The horizontal green line represents the background labeling ($0.4 \times 10^{-6}$/nm$^2$) estimated over the ultrastructural compartment that had the lowest gold density, i.e., the cytoplasm of large dendritic profiles.

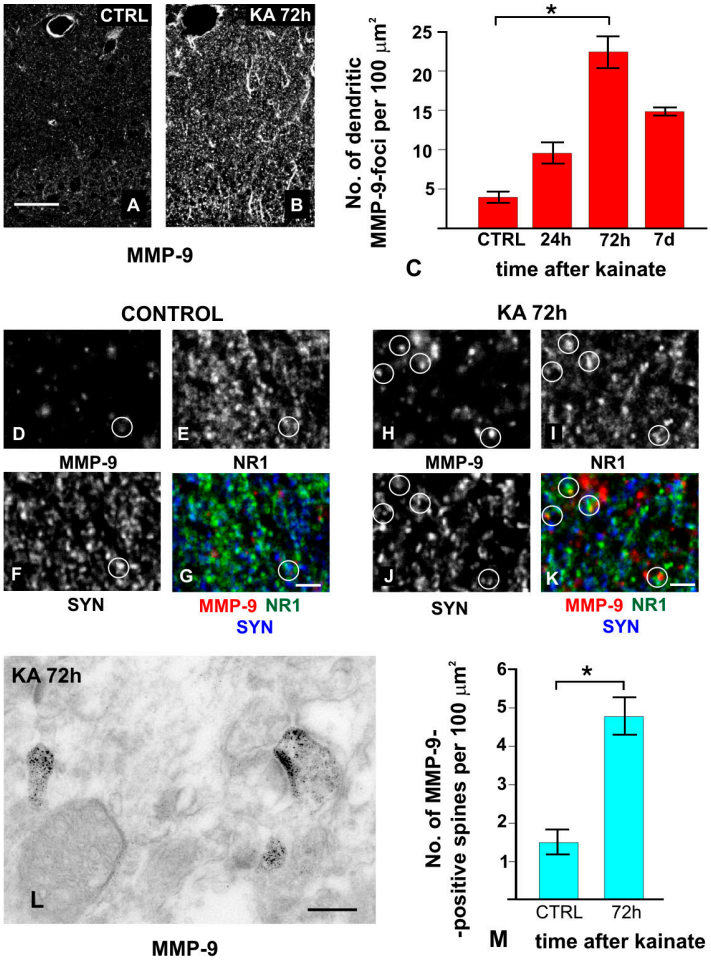


Figure 3. **MMP-9 IR after kainate treatment.** (A and B) Low-power confocal images of MMP-9 IR in the DG molecular layer in control brain (A) and 72 h after seizures (B). Bar, 75 µm. In B, note strongly increased granular IR. In addition, there is labeling of glial cells (mainly astrocytes, as indicated by their GFAP positivity; not depicted). (C) The densities of MMP-9–immunoreactive foci colocalizing with dendrites in the DG molecular layer at various time-points after seizures. Quantitative confocal evaluation of the specimens double immunostained for MMP-9 and MAP-2. Asterisk indicates significant difference (Kruskall-Wallis test; $P < 0.05$). Error bars represent SEM. (D–K) High-power view of the DG neuropil (middle molecular layer) immunostained for MMP-9 (D and H; and G and K, red), NR1 (E and I; and G and K, blue), and synaptophysin (F and J; and G and K, green) in control (D–G) and at 72 h after seizures (H–K). The number of MMP-9–positive synapses (circles, red-blue-green objects) increases prominently after kainate. The MMP-9 signal in A, B, and D–K was acquired using the photomultiplier sensitivity that was optimized to cover the maximum range of signal intensity at the 72-h time point after kainate, resulting in an apparently lower signal in controls (A and D) compared with Fig. 2. Bars, 5 µm. (L and M) Electron microscopic visualization (L) and quantification (M) of MMP-9 IR in dendritic spines in control and 72 h after seizures, using preembedding procedure with silver-enhanced diaminobenzidine. There is a prominent increase in the frequency of positive dendritic spine profiles in the sections from kainate-treated animals. Asterisk indicates statistical significance (*t* test; $P < 0.05$). Error bars represent SEM.

In contrast, when a specific MMP-9 inhibitor, S24994 (Hanessian et al., 2001), was applied after kainate, there was virtually no synaptoporin immunolabeling and, thus, apparently no sprouting (Fig. 6, C and I; and Fig. S1). Quantitative assessment of the high-resolution images of the DG revealed that MMP-9 inhibition resulted in an ~90% decrease in the density of sprouting mossy fiber terminals (Fig. 6 T). Importantly, in our experimental setup, MMP-9 inhibition had only little (if any) influence on the final extent of kainate-mediated damage (Fig. S1). Thus, we could rule out possible indirect effects of MMP-9 inhibition on sprouting/synaptogenesis, e.g., through promotion of CA3 cell survival (alleviation of triggering stimuli). Notably, although there was significant variability of neuronal damage among the cultures, the MMP-9 inhibitor was similarly effective in all of them in regard to its ability to counteract mossy fiber sprouting.

To further avoid potentially confounding effects of excitotoxic activity of kainate, we studied the effect of S24994 in cultures grown in the presence of picrotoxin (a $GABA_A$ receptor antagonist), a compound known to induce sprouting without causing cell damage (Koyama et al., 2004). Examined after 10 DIV, the cultures treated with picrotoxin had very strong punctate synaptoporin IR throughout the DG granule cell and molecular layers (Fig. 6, K and R). The overall pattern of aberrant synaptogenesis was very similar to that of kainate-treated cultures but the intensity of synaptogenesis was not as pronounced. There was no loss of MAP-2 staining, indicating absence of neurodegenerative changes (unpublished data). However, as in the experiment with kainate, picrotoxin-evoked sprouting was attenuated by administration of the MMP-9 inhibitor (Fig. 6 S).

Finally, we asked whether the reduced susceptibility of MMP-9 KO mice to PTZ kindling in vivo is associated with an attenuation of aberrant synaptogenesis. We subjected the brains of the PTZ-kindled mice to synaptoporin immunocytochemistry (Fig. 6, U and V) and found that the hippocampi of MMP-9 KO animals displayed significantly less mossy fiber synaptogenesis in the CA3 area than did hippocampi of WT mice (Fig. 6, compare U, V, and W).

## Discussion

Thus far, ion channels and receptors have been center stage in epilepsy research. Little attention has been paid to the possibility that extracellular proteinases are critically involved in the development of epilepsy. In this paper, we present the novel finding that experimental manipulations of the level and activity of MMP-9 significantly affect the susceptibility to epileptogenesis in two commonly used models of epilepsy. Most notably, lack of MMP-9 in the KO mice and overexpression of its activity in the TG rats produce opposite effects on epileptogenesis.

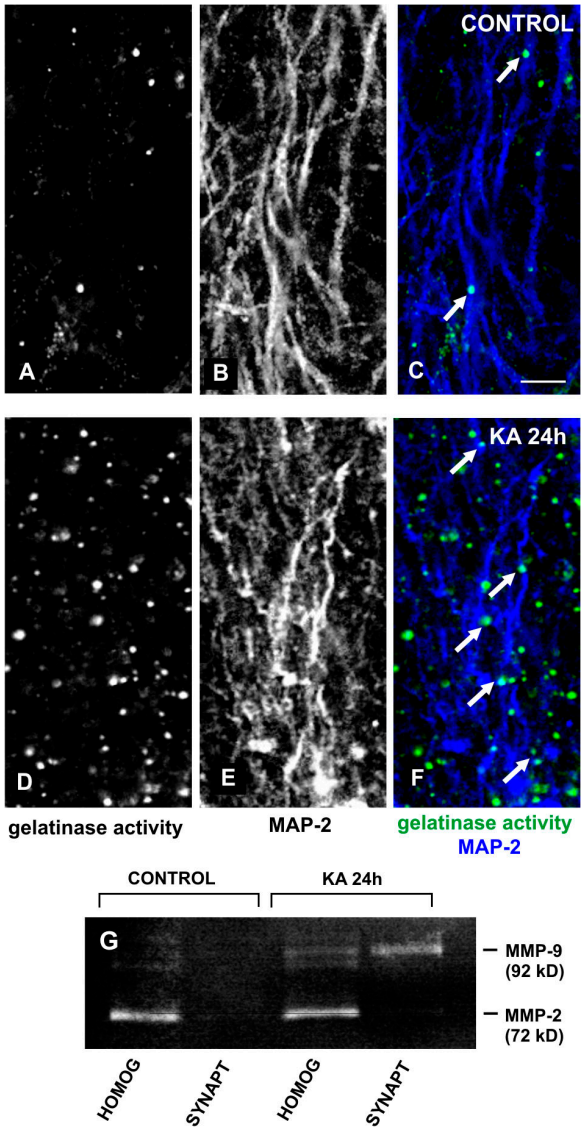


Figure 4. **Zymographic analysis of gelatinase activity.** (A–F) High-resolution fluorescence in situ zymography (A, B, D, and E, single-plane single-channel confocal images; C and F, respective overlays) shows that gelatinase foci (A and D; and C and F, green) frequently colocalize with dendrites (C and F, arrows) and are increased after kainate (compare control [A] and 24 h of kainate [KA 24 h; D]). Bar, 5 µm. (G) Gel zymography of hippocampal subcellular fractions. HOMOG, total homogenate; SYNAPT, synaptodendrosomal fraction. Top bands, MMP-9 activity; bottom band, MMP-2 activity. No MMP-9 activity is present in control synaptodendrosomes. Kainate treatment results in de novo appearance of the prominent band corresponding to synaptodendrosomal (pro–) MMP-9 activity. MMP-2 activity does not change after kainate and is absent from synaptodendrosomal fractions. The MMP-2 band should be considered as an internal control.

The MMP-9–overexpressing TG rats are reported herein for the first time. We also explore the mechanisms involved and demonstrate that the same changes in MMP-9 gene expression that regulate epileptogenesis also modify epilepsy-associated synaptic plasticity, including dendritic pruning and mossy fiber sprouting. By the use of high-resolution immunogold cytochemistry, we identified a novel synaptic pool of MMP-9 and showed that this pool increased in response to kainate treatment. Collectively, our data strongly suggest that MMP-9 plays an important role in the processes that lead to the development of recurrent epileptic seizures and the associated plasticity.

In a seminal study by Nedivi et al. (1993), TIMP1, an endogenous inhibitor of MMPs, was listed among several genes that were found to be up-regulated by kainate treatment specifically in the DG. We pursued this intriguing finding by demonstrating that TIMP1 was in fact a neuronal target of the activity-dependent transcription factor AP1 (Jaworski et al., 1999) and was up-regulated by seizures throughout the entire hippocampus. Next, while searching for a physiological significance of TIMP1 up-regulation, we found that kainate also caused a very prominent increase in neuronal MMP-9 that followed a similar spatiotemporal pattern and occurred at the levels of both gene expression and enzymatic activity (Szklarczyk et al., 2002). Although there is evidence that excitation-driven MMP-9 activation can be deleterious to neurons (Jourquin et al., 2003), this cannot apply to DG granule cells, which are known to survive even the very intense kainate-evoked status epilepticus (Sperk, 1994). Thus, we hypothesized that the prolonged MMP-9 up-regulation in the DG after status epilepticus represents an insult-related plastic response. This brings to the fore the question of what effects MMP-9 actually exerts at the cellular and subcellular levels upon its up-regulation by seizures. Because the postkainate changes occurring at the DG dendritic tree can be divided (somewhat arbitrarily) as falling into two phases, the early spine pruning and subsequent chronic progressive (aberrant) synaptogenesis, we searched for possible MMP-9 functions accordingly. Furthermore, after obtaining evidence that MMP-9 is involved in epileptogenesis in a kainate model, we investigated another model, pharmacological kindling, using TG mice and rats. Through this approach, we were able to show that the pivotal role of MMP-9 in epileptogenesis is not limited to a particular species or experimental model.

In our studies we have made extensive use of the MMP-9 KO mice. Such a model may be biased by compensatory effects, such as an overexpression of functionally related protein. Therefore, we provided additional support for our conclusions by analysis of MMP-9–overexpressing TG rats. Notably, the chemically kindled TG rats displayed a phenotype opposite to that of the MMP-9 KO mice in regard to epileptogenesis.

One could argue that the resistance of MMP-9–deficient mice to kainate-induced synaptogenesis in the DG results from their lower sensitivity to the excitotoxic action of kainate. In fact, in our initial analysis of an MMP-9–deficient mouse treated with intraamygdalar kainate injections, we noticed a considerable reduction in the extent of neurodegeneration (as compared with WT animals) at 3 wk after the kainic acid (KA) injection. However, using organotypic slice cultures, we were able to conclude that MMP-9 directly affects kainate-induced synaptogenesis, as the MMP-9 inhibitor had no effect on neuronal damage in this model yet significantly reduced mossy fiber sprouting. Our experiments with picrotoxin (which induces mossy fiber sprouting but no cell damage) support the conclusion that the effect of MMP-9 on sprouting is direct rather than mediated through an effect on cell damage. Likewise, the effect of MMP-9 on the development of epilepsy in vivo can be dissociated from any neuropathological consequences of MMP-9 KO or overexpression,

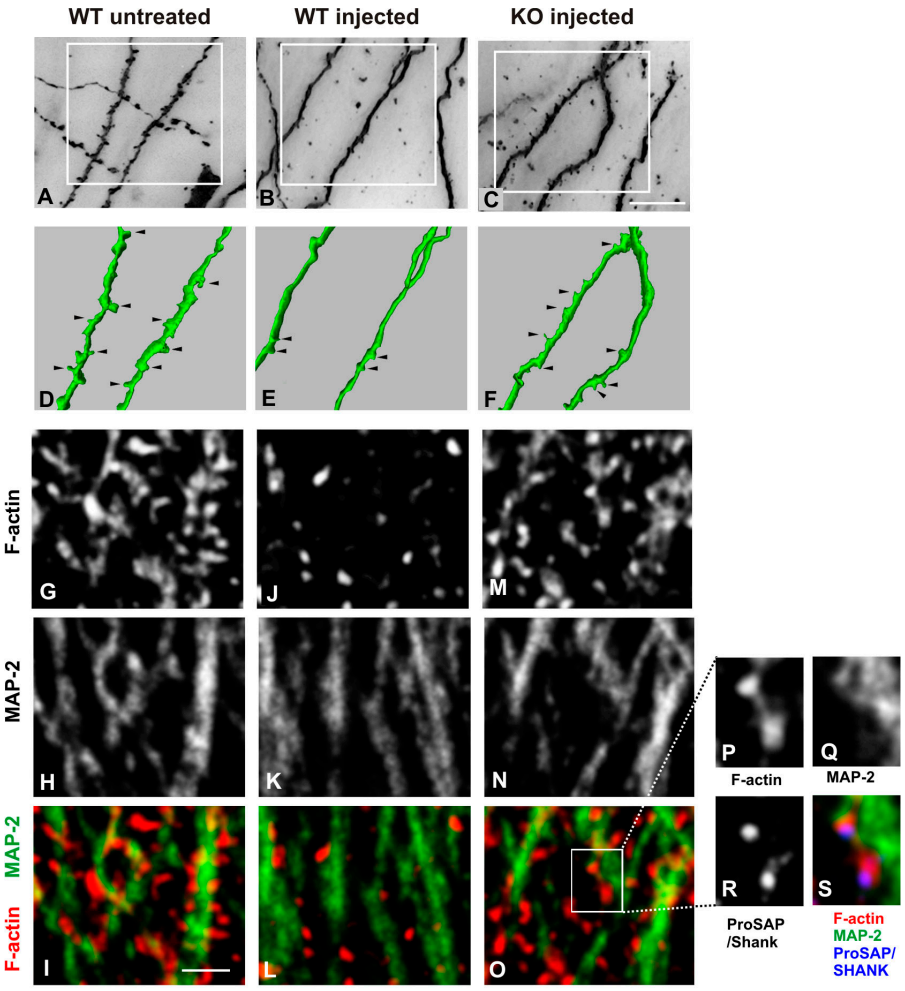


T

SPINE COUNTS

| group | WT untr. | KO untr. | WT con. | KO con. | WT inj. | KO inj. |
|---|---|---|---|---|---|---|
| spine density [per 1 μm] | 1,28 | 1,20 | 0,72 | 0,79 | 0,44 | 0,74 |
| SE | 0,03 | 0,04 | 0,04 | 0,05 | 0,03 | 0,05 |
| number of spines | 13740 | 13765 | 18170 | 14516 | 9305 | 12709 |
| number of animals | 4 | 4 | 8 | 7 | 8 | 7 |

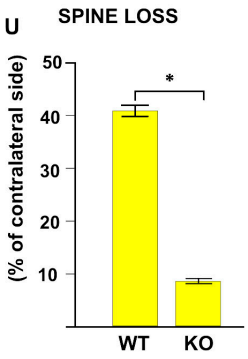


Figure 5. **The analysis and visualization of dendritic spines in MMP-9 KO and WT mice at 24 h after intraamygdalar KA injection.** (A–C) Representative fields of Golgi-stained hippocampal granule cell dendrites of the DG middle molecular layer in control (A) and kainate-treated (B and C) WT (A and B) and KO (C) mice. Bar, 50 μm. (D–F) 3D higher-resolution reconstruction of the segments shown in A–C in white rectangles. Note the striking difference in the prevalence of dendritic spines (arrowheads) between control and kainate-treated WT brain (D vs. E). Also note that the density of spines in the kainate-treated KO animal is similar to that of the untreated WT. (G–S) Representative dendritic segments from untreated (G–I) and kainate-treated (J–S) WT (J–L) and KO (M–S) animals stained with rhodamine phalloidin (red) and MAP-2 (green). Bar, 5 μm. Note that seizure-evoked loss of F-actin–positive dendritic spines (compare I and L) is virtually absent in the MMP-9 KO animal (compare I and O). (P–S) An area from O (white rectangle) showing colocalization of F-actin (red) and PSD-associated ProSAP/Shank protein (blue) that proves the identity of dendritic spines. The purple in the overlay indicates colocalization. (T and U) Dendritic spine counts (T) in untreated and injected MMP-9 WT and KO mice and estimates of dendritic spine loss (U) at the injected side (relative to the contralateral side) at 24 h after unilateral intraamygdalar kainate injection. Asterisk indicates statistical significance (*t* test; $P < 0.05$). Error bars represent SEM.

as the PTZ model (unlike the kainate model) does not show significant cell damage in the central nervous system.

Our unpublished electrophysiological observations indicate that when used alone, the specific MMP-9 inhibitor S24994 does not cause any gross changes in the electrical activity of the nervous tissue. Therefore, it is very unlikely that the effect of inhibitor was indirect, e.g., through modifying electrical epileptogenic activity. The different experimental approaches provided consistent results and are in agreement with Reeves et al. (2003), who demonstrated a beneficial effect of a general MMP inhibitor on the histological and behavioral outcome in an animal model of trauma-induced aberrant synaptic plasticity.

To determine the fine-structural localization of MMP-9, we used a variety of complementary approaches, including light and electron microscopic immunocytochemistry (with the use of two different MMP-9–specific antibodies), high-resolution in situ zymography, and subcellular fractionation. These approaches concurred to support an association of MMP-9 with dendritic spines in both naive and stimulated brain. Importantly, our electron microscopic analysis demonstrated that MMP-9 up-regulation after seizures occurred in the very same population of spines that underwent pruning (the same population was protected in MMP-9 KO). These are novel observations that force us to revise the current concepts regarding the roles of

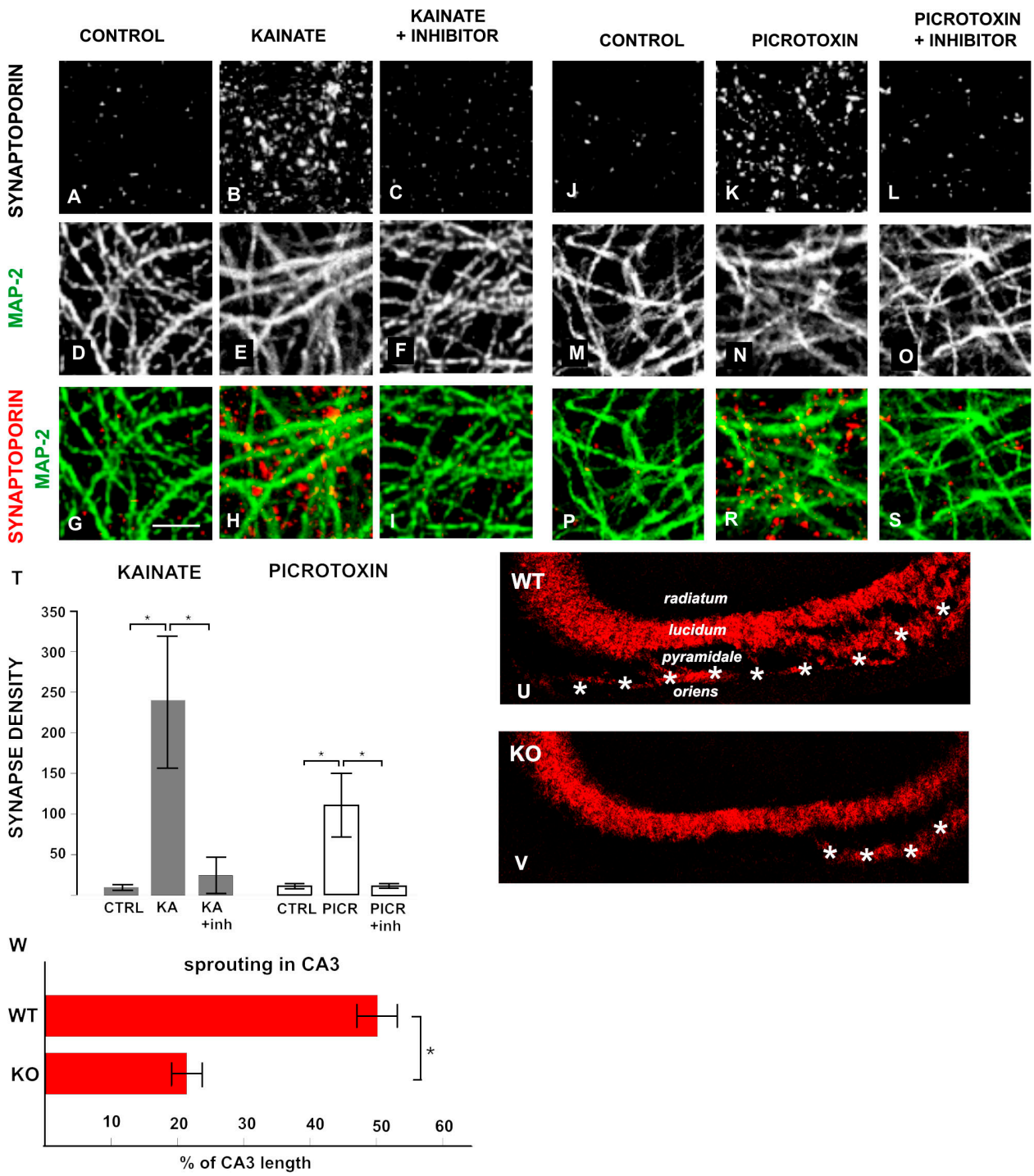


Figure 6. **MMP-9 involvement in seizure-induced synaptogenesis.** (A–S) The effect of the specific MMP-9 inhibitor S24994 on mossy fiber sprouting and aberrant synaptogenesis in the DG dendritic layer of the rat organotypic hippocampal cultures treated with either kainate (B, C, E, F, H, and I) or picrotoxin (K, L, N, O, R, and S) or untreated (A, D, G, J, M, and P). High-power confocal micrographs (A–F and J–O, single channel; G–I and P–S, respective overlays) are taken from cultures immunolabeled for synaptoporin, a mossy fibers boutons marker (A–C and J–L; and G–I and P–S, red), and MAP-2 (D–F and M–O; and G–I and P–S, green). Pharmacologic MMP-9 inhibition results in a dramatic decrease in the density of ectopic mossy fibers boutons upon both kainate (compare B and C) and picrotoxin (compare K and L) treatment. (T) Quantitative evaluation of the effect of S24994 on either kainate- (left) or picrotoxin (right)-mediated sprouting, measured as the mean number of synaptoporin-positive boutons per unit volume (30,000 $\mu m^3$) of the DG. Asterisks indicate statistical significance (*t* test; $P < 0.05$). Error bars represent SEM. (U and V) Histological effects of PTZ kindling in WT and MMP-9 KO mice. In normal animals (U), kindling is associated with a robust sprouting of mossy fibers resulting in the formation of new synapses on the basal dendrites (stratum oriens) of CA3 pyramidal cells (white asterisks), as demonstrated using confocal imaging of synaptoporin-stained (red) specimens. In contrast, there is very limited response in MMP-9–deficient animals (V). (W) Quantitative analysis of synaptoporin immunofluorescence in WT versus MMP-9 KO mice. Asterisk indicates statistical significance (Mann-Whitney *U* test; $P < 0.05$). Error bars represent SEM.

MMP-9 in synaptic plasticity, concepts which are derived mainly from functional studies and light microscopic data (Nagy et al., 2006; Bozdagi et al., 2007).

Our immunogold analysis of MMP-9 distribution in the normal hippocampus suggests that the smaller the spine, the more enzyme it contains (Fig. 2). Interestingly, recent in vivo imaging studies indicate that small spines are less stable, as they expand and collapse at much higher rates than the large ones (Matsuzaki et al., 2004). If the MMP is involved in releasing dendritic spines from constraints imposed by neighboring structures and pericellular matrix, it would be expected that small and more dynamic spines have more of it. Furthermore, small and large spine populations appear to differ from each other in their content of glutamate receptor subtypes. Large synapses (on large spines) have a higher density of AMPA than the smaller ones. In contrast, the density of NMDAR only shows modest changes with synapse size (Takumi et al., 1999). Accordingly, long-term synaptic potentiation, which is associated with transformation from silent (NMDAR only–containing) to fully excitable (NMDAR- and AMPA-containing) synapses is associated with the enlargement and/or reshaping of the dendritic spines (Toni et al., 2001; Matsuzaki et al., 2004). Notably, if these changes are precluded by the use of substances disrupting the F-actin cytoskeleton, potentiation does not occur (Fukazawa et al., 2003). It is of interest in this regard that MMP-9 appears to be involved specifically in the late phase of long-term potentiation (Nagy et al., 2006; Okulski et al., 2007). It is possible that the failure of MMP-9–deficient neurons to develop long-lasting potentiation reflected their inability to liberate spines from the milieu of pericellular matrix and cell adhesion proteins, thus curbing their expansion.

This concept would be in agreement with recent findings (Tian et al., 2007) suggesting that cleavage of a dendritic spine adhesion molecule, intercellular adhesion molecule (ICAM) 5 (telencephalin), by MMP-9 is required for activity-dependent spine enlargement. In line with our electron microscopic observations, this MMP-9 substrate was found to be present in small spines. In contrast, one could predict that mechanical constraints imposed by ECM and/or adhesion molecules (perhaps different from ICAM-5) should also impede spine pruning. Indeed, our results clearly indicate that MMP-9 is involved in kainate-induced spine pruning that shares at least some mechanisms with physiological spine-size transformations, including actin depolymerization (Fig. 1 I; Hasbani et al., 2001). Thus, it is possible that MMP-9 facilitates elimination, as well as growth of spines, through a single mechanism, i.e., facilitation of spine remodeling. 3D electron microscopic analysis, as well as functional studies in living cells, is needed to establish the precise relationship between spine size and MMP-9 contents.

At the molecular level, the mechanisms of MMP-9 action on spine dynamics remain poorly understood. Interestingly, Oray et al. (2004) have previously demonstrated that degradation of laminin (a principal component of brain ECM) by tissue plasminogen activator (tPA) directly impacts the dynamics of dendritic spines. MMP-9 could be involved because laminin is one of its substrates and tPA is known to act upstream of MMP-9 (Sternlicht and Werb, 2001). Cadherins and integrins are two major families of synaptic adhesion proteins that have been strongly implicated in spine physiology (Benson et al., 2000). Outside the brain, members of these families are known to function as either MMP substrates or receptors (Sternlicht and Werb, 2001). The role of integrins in MMP-9–mediated synaptic plasticity is strongly supported by the finding that MMP-9–mediated long-term potentiation depends on intact integrin function (Nagy et al., 2006). Finally, as found by Tian et al. (2007), ICAM-5 is an MMP-9 substrate involved directly in spine dynamics. However, besides the proposed role in structural plasticity, MMP-9 could cleave and thereby activate (or inhibit) other molecules involved in functional plasticity. This would be similar to the action of tPA toward pro–brain-derived neurotrophic factor (Pang et al., 2004). Notably, pro–brain-derived neurotrophic factor is an MMP substrate as well (Sternlicht and Werb, 2001). Finally, similar to serine proteinases (Fernandez-Monreal et al., 2004; Kvajo et al., 2004), a proteolytic action of MMP-9 could be directly involved in some aspects of signal transmission (Michaluk and Kaczmarek, 2007).

The second major phenomenon that we describe in this paper is MMP-9 action in aberrant synaptogenesis that occurs in the hippocampal DG days to weeks after status epilepticus and in the CA3 area upon kindling. Seizure-induced synaptogenesis is not associated with pruning but with an increase in spine number (Suzuki et al., 1997; Isokawa, 2000) and/or size (Represa et al., 1993). However, because both synapse elimination and formation likely require the same proteolytic degradation of extracellular matrix and/or adhesion molecules, it is, in fact, not unreasonable to hypothesize that MMP-9 is involved in both aforementioned phenomena. If this is true, blocking MMP-9 at the stage of mossy fiber sprouting should prevent accompanying spine proliferation, thereby decreasing the efficiency of synaptogenesis as, indeed, happens in KO mice (Fig. 6). In contrast, MMP-9 overexpression at this stage could facilitate spine proliferation, thus stimulating formation of the new aberrantly positioned synapses. Experiments that aim to verify the latter prediction in TG rats are in progress in our laboratory.

We cannot exclude the possibility that under some conditions, e.g. during sprouting and synaptogenesis, MMP-9 acts on the presynaptic domain, including axonal growth cones, as suggested by some cell culture studies (Shubayev and Myers, 2004). Finally, it is also possible that MMP-9 exerts its influence on synaptogenesis after being released from glial cells. Indeed, the presence of MMP-9 in astrocytes (by double labeling with GFAP; Szklarczyk et al., 2002) and in oligodendrocytes under nonstimulated conditions (Oh et al., 1999) has been previously described. Furthermore, our ultrastructural immunolocalization, as well as electron microscopic in situ hybridization data (Konopacki et al., 2007), consistently indicates the presence of the enzyme in the tiny astrocytic processes that ensheath the synapses. This allows for the fascinating possibility that several pools of MMP-9 contribute to the synaptic effects of this enzyme. The specific roles of these MMP-9 reservoirs, as well as the modes of their regulation, are currently a subject of study in our laboratory. With respect to epileptogenesis, we found the highest level of MMP-9 expression in astrocytes at the 7th d after kainate, i.e., exactly when sprouting is most likely to be initiated

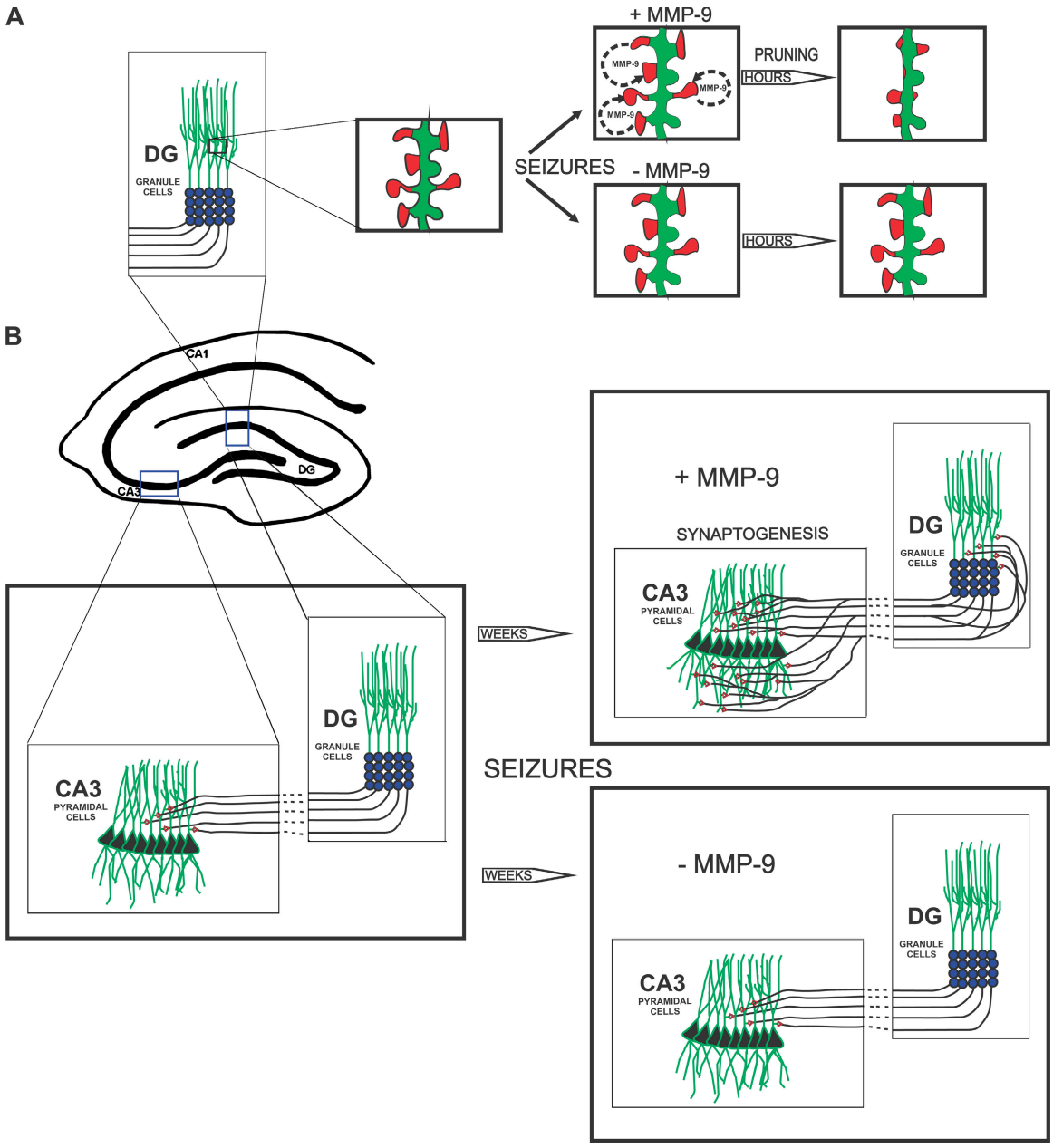


Figure 7. **Schematic representation of presumable MMP-9 action in hippocampal epileptogenesis based on the present study.** (A) Status epilepticus induces dendritic spine pruning in the DG molecular layer. This is mediated by MMP-9 released from spines upon the seizures. In the absence of MMP-9, the pruning is attenuated, despite the presence of adequate stimulus. (B) Sprouting of mossy fibers and aberrant synaptogenesis in the hippocampal epileptogenesis involve MMP-9 because both of these phenomena do not develop in the absence of the enzyme.

(Fig. 3 and not depicted). Although MMP-9 of astrocytic origin may contribute to epileptogenesis, our studies in animals with MMP-9 overexpression (in neurons) suggest that the neuronal pool of MMP-9 is the more important, (Fig. S3, available at http://www.jcb.org/cgi/content/full/jcb.200708213/DC1).

A key question is whether MMP-9 influence on spine dynamics and synaptogenesis, can explain how the enzyme facilitates the long-term aberrant plastic changes subserving the development of epilepsy. There is a near consensus that sprouting, even if not absolutely required for the TLE to develop, powerfully stimulates epileptogenesis by generating recurrent excitatory circuits within the hippocampal formation (for review see Morimoto et al., 2004). Thus, we believe that it is the effect on pathological synaptogenesis that underlies the role of MMP-9 in the progression of epilepsy (Fig. 7). Our data indicate that the role of MMP-9 in aberrant synaptogenesis involves its action on dendritic spines (Fig. 7), although further studies are needed to confirm this.

In a wider neurobiological context, our results place MMP-9 in the very small group of extracellular proteinases that function at the synapses. These are mainly serine proteinases, such as tPA, neuropsin, neurotrypsin, and possibly also thrombin (for review see Shiosaka, 2004). Among MMPs, only MMP-7 and MMP-24 have been added to this group so far (Bilousova et al., 2006;

Monea et al., 2006; for review see Ethell and Ethell, 2007). Notably, all these enzymes appear to be involved in some aspects of synaptic plasticity. Besides being engaged in normal processes, tPA and neuropsin were implicated in the pathogenesis of epilepsy (Wu et al., 2000; for review see Shiosaka, 2004). It remains to be determined if, and how, these enzymes interact with one another in health and disease, e.g., whether presynaptic tPA can function as an activator of postsynaptic MMP-9.

We would like to propose that our data have direct implications for human TLE. In fact, behavioral, anatomical, and molecular events that are associated with kainate- and kindling-induced epileptogenesis in rats and mice largely reproduce the corresponding events in human TLE (Ben-Ari, 2001). An essential feature of the human disease captured by both models is aberrant synaptic plasticity. In this paper, we show that the formation of aberrant synaptic networks depends on MMP-9. Because these networks keep progressing, contributing to the increasing severity of the disease, the inhibition of this process might be beneficial at any stage. Hence, this work is not only a step toward understanding pathophysiology of epilepsy but also offers an opportunity to search for novel therapeutic approaches targeting the mechanisms of this disease.

## Materials and methods

### Animals

Experiments were performed on adult male Wistar rats and on adult MMP-9 KO mice C57BL/6 strain (provided by Z. Werb, University of California, San Francisco, San Francisco, CA; Vu et al., 1998), all according to the rules established by the Ethical Committee on Animal Research of the Nencki Institute, based on national laws that are in full agreement with the European Union directive on animal experimentation.

### Generation of MMP-9–overexpressing rats

Expression vector with autoactive MMP-9 gene driven by synapsin-1 promoter were constructed in our laboratory. Plasmid DNA for microinjection was purified using the plasmid maxiprep method. The expression cassette was prepared by digesting the vector DNA with PacI and XbaI enzymes and microinjecting it into fertilized eggs of Wistar rats (Fig. S1). All rats were raised and maintained under specific pathogen-free conditions. Genomic DNA was extracted from the offspring by ear biopsy and founders were identified by PCR. The primer sequences for the PCR were 5′-AGG CGC GCT GAC GTC ACT CG-3′ and 5′-CGC GCT CCACAG TGC GAA-3′. PCR reactions were performed for 30 cycles at 94°C for 45 s, 59°C for 60 s, and 72°C for 60 s. Two independent lines of TG rats were generated.

### Kainate treatment

Kainate (Ocean Produce) was used in both rat and mice experiments. Status epilepticus in rats was induced by intraperitoneal injection of 10 mg/kg and the animals were observed for up to 6 h, as previously described (Szklarczyk et al., 2002).

The adult male mice were anesthetized with 1.3 ml/kg ketamine and 1.25 ml/kg xylazine and subjected to stereotactic unilateral injection with 1 nmol kainate in 0.3 µl PBS into the amygdala (Wu et al., 2000). The coordinates of the injection were the following: bregma, 1.6 mm; medial–lateral, 3.3 mm; and dorsoventral, 4.5 mm. The kainate was delivered over 30 s. The injection needle remained at the injection coordinates for another 2 min afterward to prevent reflux of fluid.

For immunocytochemical studies, animals were lethally anesthetized and perfused transcardially with a fixative (4% formaldehyde, freshly depolymerized from PFA, in PBS; in some electron microscopic experiments, 0.1% glutaraldehyde was added). Brains were removed, postfixed in the same fixative, and either processed for paraffin embedding or cryoprotected and snap frozen in isopentane cooled on dry ice.

For biochemical studies, the brains were removed immediately after decapitation. From each brain, hippocampi were dissected, frozen on dry ice, and stored until assayed.

### PTZ kindling

Mice received intraperitoneal injections of 30–40 mg/kg PT every other day consecutively for 6 wk (De Sarro et al., 2004). Behavioral seizures were scored according to a modified scale of Racine: 0, no behavioral changes; 1, facial movements and ear and whisker twitching; 2, myoclonic convulsions without rearing; 3, myoclonic convulsions with rearing; 4, clonic convulsion with loss of posture; and 5, generalized clonic-tonic seizures or death. The brains of mice that died during experiments, as well as of those that were killed after the termination of experiments, were immersion fixed in 4% PFA and stored in PBS plus 0.1% sodium azide until further processing. Subsequent immunocytochemical procedures were performed as described in the previous section.

Rats received subcutaneous injections of 40 mg/kg PTZ every other day consecutively for 8 wk and were behaviorally scored using the same scale as for mice. In addition, another group of rats was treated to the intraperitoneal injections of PTZ.

### Organotypic hippocampal culture and kainate and picrotoxin treatment

Cultures of hippocampal slices were prepared essentially according to Jourquin et al. (2003). In brief, 8–10-d-old rat pups were decapitated and the hippocampi were rapidly dissected on a cold plate. 400-µm-thick slices, perpendicular to hippocampal long axis, were cut with a tissue chopper and plated (three to four per well) onto Millicel-CM biomembranes (Millipore). The slices were cultured in a humidified incubator at 37°C with 5% $CO_2$. Kainate was added to some for 24 h on DIV5 at a 10-µM concentration, and the cultures were fixed on DIV20 and processed for immunocytochemical stainings. In the case of picrotoxin, the compound was present in culture medium at concentration of 100 µM throughout the whole culturing period (Koyama et al., 2004). MMP-9 inhibition was achieved by growing the cultures in the presence of the specific MMP-9 inhibitor S24994 (Hanessian et al., 2001) at a 100-nM concentration. The inhibitor was either present from the beginning (picrotoxin experiment) or added on DIV6 (immediately after removal of kainate).

### Immunocytochemical procedures

**Primary antibodies.** Two rabbit polyclonal anti–MMP-9 antibodies were used: an antibody raised against the catalytic domain of the rat MMP-9 (Torrey Pines Biolabs, Inc.; Szklarczyk et al., 2002) and an antibody raised against the epitope comprising the catalytic domain of the mouse enzyme (gift from R. Senior, Washington University, St. Louis, MO; Betsuyaku et al., 2000; see subsequent sentences for working dilutions). Both antibodies recognize active and latent forms of MMP-9 (Betsuyaku et al., 2000; Szklarczyk et al., 2002). The following mouse marker antibodies were used for double and triple immunofluorescent stainings: anti–MAP-2, a dendritic marker, diluted at 1:200 (Millipore); anti-synaptophysin, a presynaptic marker, diluted at 1:20 (Dako); and anti–NMDAR subunit NR1 and anti–GABA-AR subunits β2/3, postsynaptic markers, both diluted at 1:50 (Millipore). Sprouting mossy fiber terminals were visualized using a rabbit anti-synaptoporin antiserum (Synaptic Systems GmbH; Singec et al., 2002) diluted at 1:200.

**Light microscopic immunocytochemistry.** Light microscopic immunocytochemistry was performed essentially according to Boeckers et al. (1999) in either 50-µm-thick free-floating sections of frozen tissues or 4-µm-thick paraffin sections. The latter were used in studies of MMP-9 colocalization with NR1 NMDAR or GABA-AR because of their permeability and mechanical resistance to antigen retrieval techniques. In such experiments, antigen retrieval steps using 0.1% pepsin and microwaving were necessary and were done immediately after deparaffinization. Both kinds of sections were subjected to standard blocking steps, including, if needed, blocking of endogenous biotin (Avidin/Biotin Blocking kit; Vector Laboratories), followed by overnight incubation in the anti–MMP-9 antibody, diluted at 1:2,000 (R. Senior) or 1:200 (Torrey Pines Biolabs, Inc.). The detection of immunoreactions was performed using either species-specific secondary antibodies directly conjugated to fluorophores or biotinylated secondary antibody (Vector Laboratories) followed by a fluorophore-conjugated streptavidin (Invitrogen). For double or triple stainings, we used antibodies (or streptavidin) conjugated to green Alexa 488 (Invitrogen), red Cy3 (Jackson ImmunoResearch Laboratories), or near-infrared Cy5 fluorophores (Jackson ImmunoResearch Laboratories). In the case of anti–MMP-9, an amplification step using biotinylated tyramide (PerkinElmer) was included in avidin-biotin–based detection. For triple immunofluorescence with two marker antibodies originating from the same species, we used Zenon, a custom antibody-(immuno)labeling system (Invitrogen).

For negative controls, the primary antibody was omitted, replaced by a nonimmune IgG, and preabsorbed with the target antigen. In double

or triple immunostainings, special care was taken to control for any possible cross-reactivity of the detection systems.

**Fluorescent imaging.** Fluorescent specimens were examined under a spectral confocal microscope (TCS SP2; Leica), using 488 nm Ar, 543 nm GeNe, and 633 nm HeNe laser lines for the excitation of Alexa 488, Cy3, and Cy5, respectively. The images were acquired through the internal TCS SP2 detectors/photomultipliers. To avoid cross talk between the fluorophores, we carefully adjusted the spectral ranges of detectors and scanned images sequentially. The Plan Apo oil-immersion objective lenses were 40× (1.25 NA), 63× (1.32 NA), and 100× (1.4 NA). The images in Figs. 2 (C and H–P), 5 (G–S), and 6 (A–S) were 3D deconvolved by means of Huygens Professional software (Scientific Volume Imaging), using classical maximum likelihood algorithm and theoretical point-spread functions. For final inspection, the images were processed using Photopaint (Corel). Brightness and contrast adjustments and/or Gaussian smoothing were applied, if necessary, to improve image clarity. Quantitative analyses of immunofluorescence results included unbiased morphometric evaluation using ImageJ software (National Institutes of Health) and are listed in the following paragraphs.

We quantified MMP-9–positive puncta colocalizing with dendrites. The analysis of MMP-9 (red channel)–MAP-2 (green channel) colocalization in the DG of control and kainate-treated rats was performed in single-plane confocal images acquired using a 63× objective (oil immersion; 1.3 NA) with a zoom factor of four. The settings of photomultipliers were adjusted to obtain the maximal dynamic ranges of pixels in each channel. Because the intensity of MMP-9 staining (red channel) differed considerably among the time points, several trials were performed before the optimal value was found. However, even with the optimized setting, we could not avoid considerable pixel saturation at 72 h after kainate. Thus, at this time point the sensitivity of the photomultiplier was decreased by 10%. Otherwise, identical scanning conditions were maintained during all image acquisition sessions, including the constant distance of the focal plane to the surface of the section (7 µm). In each brain, three different random focal planes were scanned in each of the molecular layer subdivisions, inner, medial, and outer. We designed a macro within ImageJ that automatically segmented areas in which red and green signals colocalized. The colocalization was considered to occur if, at a given pixel, both signals were above the threshold values (red, 115; green, 70) and their ratio of signal intensities was >0.33. Using an unbiased counting frame (Gundersen, 1978), at each time point we estimated the mean number of colocalizing objects per unit area of the tissue, the ratio of the number of colocalizing objects to the number of all MMP-9–immunoreactive objects, and the mean fluorescence intensity of the colocalizing objects, defined as the product of the mean area of the colocalizing objects times the mean brightness (red channel). At least four animals were analyzed at each time point. Statistical analysis was performed using Kruskall-Wallis ANOVA with the level of significance defined as $P < 0.05$.

We quantified mossy fiber synapses in hippocampal organotypic cultures. The measurements were performed in cultures (prepared as described in Organotypic hippocampal culture...) stained with the anti-synaptoporin antibody followed by the anti–rabbit Cy3 (Jackson ImmunoResearch Laboratories) secondary. The fluorophore was excited with 543 laser light, and stacks of 7–25 confocal planes were acquired using a 40× objective (oil immersion; 1.25 NA). Three different fields covering the area of granule cell plus molecular layers were acquired from each culture. The stacks were analyzed using an automatic 3D analysis function of ImageJ at the threshold of 101. The results were calculated as numbers of mossy fiber boutons per 30,000 $\mu m^3$. Statistical analysis was performed using *t* test with the level of significance defined as $P < 0.05$.

We performed confocal analysis of dendritic spine density. Dendritic spines were identified using a guinea pig anti-ProSAP2/Shank antibody and a PSD marker (Boeckers et al., 1999) together with rhodamine-phalloidin (Sigma-Aldrich), which binds to spine F-actin, or with a guinea pig anti-drebrin antibody (Fitzgerald). The measurements were performed in single-plane confocal images acquired using a 100× objective (oil immersion; 1.4 NA) with a zoom factor of four. Spines (rhodamine, red channel) and dendrites (Cy5, blue channel) were scanned sequentially using laser lines of 543 and 633 nm, respectively. The settings of photomultipliers were adjusted to obtain the maximal dynamic ranges of pixel intensities in each channel. Identical scanning conditions were maintained during all image acquisition sessions. In each section the position of focal plane was set at the level of maximum intensity of the blue channel. From each hippocampus, three different random fields were scanned within the middle molecular layer. The number of spines and the total length of dendritic segments within each unbiased counting frame were measured automatically using a custom-designed ImageJ macro. As a result, an estimate of the dendritic spine linear density (per 1 µm of the dendritic length) was obtained for each group. Statistical analysis was performed using *t* test with the level of significance defined as $P < 0.05$.

**Electron microscopic immunocytochemistry.** Preembedding technique was used according to Boeckers et al. (1999). In brief, the brains were perfusion fixed with 4% PFA (plus 0.1% gluteraldehyde in the case of anti–MMP-9) and immunostained free floating just as for light microscopy, except that repeated freezing thawing was applied at the permeabilization step instead of Triton X-100 and peroxidase-based detection was used with DAB as a chromogen. The sections were subjected to silver enhancement and processed for electron microscopy as previously described (Boeckers et al., 1999). The specimens were examined under an electron microscope (912; Carl Zeiss, Inc.) equipped with a spectroscopic filter (Omega Optical) and a charge-coupled device camera (2K; Gatan) operating at 80 kV.

Postembedding procedure was performed according to Mathiisen et al. (2006). In brief, normal Wistar rats were perfused transcardially with a fixative consisting of 4% formaldehyde plus 0.1% glutaraldehyde. The brains were postfixed in the same fixative, cut into 0.5–1.0-mm slices, cryoprotected, snap frozen in liquid propane (−170°C), and subjected to freeze substitution in an apparatus (EM AFS; Leica). Specimens were then embedded in Lowicryl HM20 resin, polymerized by UV light at −45–0°C, and cut into ultrathin sections. The immunoreactions consisted of sequential incubations with a rabbit anti–MMP-9 antibody (Torrey Pines Biolabs, Inc.) diluted at 1:50, followed by species-specific goat secondary antibodies coupled to 10-nm gold particles (GE Healthcare). The specimens were examined with an electron microscope (CM-10; Philips) at 60 kV. Images were acquired using either a charge-coupled device camera (1K; Soft Imaging System) or photographic plate camera. In the latter case, negatives were digitized at a 1,200-dpi resolution using a flatbed scanner (BearPaw; Mustek). Final adjustments of image brightness and contrast were performed using Photopaint. The sizes of, and gold particle densities within, various ultrastructural compartments were measured in digital micrographs using ImageJ (either manually or automatically). As a background, we assumed the labelling over the cytoplasm of the large dendritic profiles, which was the lowest among all compartments. Such an estimate is likely to be a slight overestimate of the true background labelling (Mathiisen et al., 2006). The statistical evaluation of the labelling was performed using the $\chi^2$ test and observed and expected gold counts over the given compartments (Mayhew et al., 2003).

### Golgi impregnation

Mouse brains were perfusion fixed using 4% PFA in PBS, immersed in 5% potassium dichromate for 4 d, immersed in 1% silver nitrate for 4 d, embedded in celloidin, and cut into 200-µm-thick sections. Dendritic spines were counted manually in image stacks obtained using a microscope equipped with a motorized stage and a 60× objective lens (1.25 NA). The counting was performed in the DG middle molecular layer (dendritic segments from at least three different cells) of four untreated and six KA-injected animals of either genotype. In the injected mice, both affected and contralateral hippocampi were evaluated. The results were evaluated using *t* test with the level of significance defined as $P < 0.05$.

### Isolation of synaptosomes

Isolation of synaptosomes was performed according to Havik et al. (2003). In brief, frozen tissue was melted, homogenized in a glass homogenizer, and subjected to a series of centrifugations that yielded P1 (cell debris and nuclei), P2 (crude synaptosomes/mitochondria), P3 (microsomes), and S (cytosol) fractions. The P2 fraction was further separated into myelin, membranes/Golgi, and synaptosomes using a discontinuous sucrose density gradient (0.8/1.0/1.2 M).

### Gel zymography

The assay was performed according to Szklarczyk et al. (2002), using gelatin–Sepharose 4B (GE Healthcare) and 8% polyacrylamide gel containing 5 mg/ml of gelatin (Loba Feinchemie) for enzyme purification and detection, respectively. Data were collected using the gel documentation program Gene Snap (InGenius) and Bio Imaging System (Syngen, Inc.) and pictures were prepared using Photoshop (Adobe).

### In situ zymography

We first used established techniques of in situ zymography in which a quenched fluorescent substrate (DQ gelatin) is applied to fresh-frozen tissue sections (Oh et al., 1999; Jourquin et al., 2003). This approach, however, was totally unsatisfactory because tissue integrity was very poorly preserved, which was evident at the high magnifications required to visualize

individual dendrites. To overcome this problem, we took advantage of the technique widely used in electrophysiological studies, in which slices of fresh brain are cut and subsequently maintained at conditions that allow preservation of at least some features of the living tissue for a definite time. The refined procedure used 150-µm-thick fresh brain vibratome sections that were placed in tissue culture wells and covered with a solution of 50 mg/ml DQ gelatin (Invitrogen) diluted in artificial cerebrospinal fluid of the following composition: 117 mM NaCl, 1.2 mM $MgSO_4$, 4.7 mM KCl, 2.5 mM $CaCl_2$, 25 mM $NaHCO_3$, 1.2 mM $NaH_2PO_4$, and 10 mM glucose. The specimens were kept for 2 h at 37°C with 5% $CO_2$ in a tissue culture incubator, rinsed twice with PBS for 10 min at RT, and fixed overnight with 4% PFA in PBS. Subsequent coimmunostaining for visualization of dendrites was performed essentially as described in Light microscopic immunocytochemistry, except that the step of the slice dehydration-rehydration using acetone/methanol solution was included at the beginning of the staining to help tissue permeabilization. The examination of the sections under the confocal microscope indicated that the procedure gave acceptable results in terms of both retaining enzymatic activity and tissue integrity.

**Online supplemental material**

Fig. S1 presents the outline, as well as the biochemical validation, of the procedure of making TG rats that overexpress MMP-9. Fig. S2 shows confocal micrographs demonstrating colocalization of MMP-9 and the dendritic spine marker drebrin. Fig. S3 shows low power confocal micrographs of the hippocampal organotypic cultures demonstrating the effect of pharmacological inhibition of MMP-9 on kainate-induced mossy fibers sprouting (in both supra- and infragranular layer [Frotscher et al., 2000]). Online supplemental material is available at http://www.jcb.org/cgi/content/full/jcb.200708213/DC1.

We are very grateful to Dr. Z. Werb (University of California, San Francisco, San Francisco, CA) for providing us with MMP-9 KO animals. We are also very grateful to Dr. R. Senior for his generous gift of the anti–MMP-9 antibody. We thank Dr. A. Wrzosek and L. Kilianek for their help with the confocal microscope. We also thank Drs. M. Khrestchatisky and S. Rivera (Mediterranean University, Marseille, France) for their helpful comments on in situ zymography.

This work was supported by KBN (State Committee for Scientific Research; grants 3 P05A 022 24 to G.M. Wilczynski and PBZ-MIN-005/P04/2002 to L. Kaczmarek), The Wellcome Trust (D.C. Gorecki and L. Kaczmarek), The International Centre for Genetic Engineering and Biotechnology (L. Kaczmarek), and Glutamate Receptor Interacting Proteins As Novel Neuroprotective Targets (GRIPANNT; L. Kaczmarek and O.P. Ottersen).

Submitted: 31 August 2007
Accepted: 7 February 2008

## References

Bannikov, G.A., T.V. Karelina, I.E. Collier, B.L. Marmer, and G.I. Goldberg. 2002. Substrate binding of gelatinase B induces its enzymatic activity in the presence of intact propeptide. *J. Biol. Chem.* 277:16022–16027.

Ben-Ari, Y. 2001. Cell death and synaptic reorganizations produced by seizures. *Epilepsia.* 42:5–7.

Benson, D.L., L.M. Schnapp, L. Shapiro, and G.W. Huntley. 2000. Making memories stick: cell-adhesion molecules in synaptic plasticity. *Trends Cell Biol.* 10:473–482.

Betsuyaku, T., Y. Fukuda, W.C. Parks, J.M. Shipley, and R.M. Senior. 2000. Gelatinase B is required for alveolar bronchiolization after intratracheal bleomycin. *Am. J. Pathol.* 157:525–535.

Bilousova, T.V., D.A. Rusakov, D.W. Ethell, and I.M. Ethell. 2006. Matrix metalloproteinase-7 disrupts dendritic spines in hippocampal neurons through NMDA receptor activation. *J. Neurochem.* 97:44–56.

Boeckers, T.M., M.R. Kreutz, C. Winter, W. Zuschratter, K.H. Smalla, L. Sanmarti-Vila, H. Wex, K. Langnaese, J. Bockmann, C.C. Garner, and E.D. Gundelfinger. 1999. Proline-rich synapse-associated protein-1/cortactin binding protein 1 (ProSAP1/CortBP1) is a PDZ-domain protein highly enriched in the postsynaptic density. *J. Neurosci.* 19:6506–6518.

Bozdagi, O., V. Nagy, K.T. Kwei, and G.W. Huntley. 2007. In vivo roles for matrix metalloproteinase-9 in mature hippocampal synaptic physiology and plasticity. *J. Neurophysiol.* 98:334–344.

Chen, Z.L., and S. Strickland. 1997. Neuronal death in the hippocampus is promoted by plasmin-catalyzed degradation of laminin. *Cell.* 91:917–925.

De Sarro, G., G.F. Ibbadu, R. Marra, D. Rotiroti, A. Loiacono, E. Donato Di Paola, and E. Russo. 2004. Seizure susceptibility to various convulsant stimuli in dystrophin-deficient mdx mice. *Neurosci. Res.* 50:37–44.

Engel, J. Jr. 1996. Epilepsy: structural or functional? *AJNR Am. J. Neuroradiol.* 17:243–244.

Ethell, I.M., and D.W. Ethell. 2007. Matrix metalloproteinases in brain development and remodeling: Synaptic functions and targets. *J. Neurosci. Res.* 85:2813–2823.

Fernandez-Monreal, M., J.P. Lopez-Atalaya, K. Benchenane, M. Cacquevel, F. Dulin, J.P. Le Caer, J. Rossier, A.C. Jarrige, E.T. Mackenzie, N. Colloc'h, C. Ali, and D. Vivien. 2004. Arginine 260 of the amino-terminal domain of NR1 subunit is critical for tissue-type plasminogen activator-mediated enhancement of *N*-methyl-D-aspartate receptor signaling. *J. Biol. Chem.* 279:50850–50856.

Frotscher, M., A. Drakew, and B. Heimrich. 2000. Role of afferent innervation and neuronal activity in dendritic development and spine maturation of fascia dentata granule cells. *Cereb. Cortex.* 10:946–951.

Fukazawa, Y., Y. Saitoh, F. Ozawa, Y. Ohta, K. Mizuno, and K. Inokuchi. 2003. Hippocampal LTP is accompanied by enhanced F-actin content within the dendritic spine that is essential for late LTP maintenance in vivo. *Neuron.* 38:447–460.

Gundersen, H.J. 1978. Estimators of the number of objects per area unbiased by edge effects. *Microsc. Acta.* 81:107–117.

Hanessian, S., N. Moitessier, C. Gauchet, and M. Viau. 2001. N-Aryl sulfonyl homocysteine hydroxamate inhibitors of matrix metalloproteinases: further probing of the S(1), S(1)', and S(2)' pockets. *J. Med. Chem.* 44:3066–3073.

Hasbani, M.J., N.M. Viquez, and M.P. Goldberg. 2001. NMDA receptors mediate hypoxic spine loss in cultured neurons. *Neuroreport.* 12:2731–2735.

Havik, B., H. Rokke, K. Bardsen, S. Davanger, and C.R. Bramham. 2003. Bursts of high-frequency stimulation trigger rapid delivery of pre-existing alpha-CaMKII mRNA to synapses: a mechanism in dendritic protein synthesis during long-term potentiation in adult awake rats. *Eur. J. Neurosci.* 17:2679–2689.

Isokawa, M. 2000. Remodeling dendritic spines of dentate granule cells in temporal lobe epilepsy patients and the rat pilocarpine model. *Epilepsia.* 41:S14–S17.

Jaworski, J., I.W. Biedermann, J. Lapinska, A. Szklarczyk, I. Figiel, D. Konopka, D. Nowicka, R.K. Filipkowski, M. Hetman, A. Kowalczyk, and L. Kaczmarek. 1999. Neuronal excitation-driven and AP-1-dependent activation of tissue inhibitor of metalloproteinases-1 gene expression in rodent hippocampus. *J. Biol. Chem.* 274:28106–28112.

Jourquin, J., E. Tremblay, N. Decanis, G. Charton, S. Hanessian, A.M. Chollet, T. Le Diguardher, M. Khrestchatisky, and S. Rivera. 2003. Neuronal activity-dependent increase of net matrix metalloproteinase activity is associated with MMP-9 neurotoxicity after kainate. *Eur. J. Neurosci.* 18:1507–1517.

Konopacki, F.A., M. Rylski, E. Wilczek, R. Amborska, D. Detka, L. Kaczmarek, and G.M. Wilczynski. 2007. Synaptic localization of seizure-induced matrix metalloproteinase-9 mRNA. *Neuroscience.* 150:31–39.

Koyama, R., M.K. Yamada, S. Fujisawa, R. Katoh-Semba, N. Matsuki, and Y. Ikegaya. 2004. Brain-derived neurotrophic factor induces hyperexcitable reentrant circuits in the dentate gyrus. *J. Neurosci.* 24:7215–7224.

Kvajo, M., H. Albrecht, M. Meins, U. Hengst, E. Troncoso, S. Lefort, J.Z. Kiss, C.C. Petersen, and D. Monard. 2004. Regulation of brain proteolytic activity is necessary for the in vivo function of NMDA receptors. *J. Neurosci.* 24:9734–9743.

Mathiisen, T.M., E.A. Nagelhus, B. Jouleh, R. Torp, D.S. Frydenlund, M.-N. Mylonakou, M. Amiry-Moghaddam, L. Covolan, J.K. Utvik, B. Riber, et al. 2006. Postembedding immunogold cytochemistry of membrane molecules and amino acid transmitters in the central nervous system. *In* Neuroanatomical Tract-Tracing. L. Zaborszky, F.G. Wouterlood, and J.L. Lanciego, editors. Springer US, New York. 72–108.

Matsuzaki, M., N. Honkura, G.C. Ellis-Davies, and H. Kasai. 2004. Structural basis of long-term potentiation in single dendritic spines. *Nature.* 429:761–766.

Mayhew, T., G. Griffiths, A. Habermann, J. Lucocq, N. Emre, and P. Webster. 2003. A simpler way of comparing the labelling densities of cellular compartments illustrated using data from VPARP and LAMP-1 immunogold labelling experiments. *Histochem. Cell Biol.* 119:333–341.

McKhann, G.M. II, H.J. Wenzel, C.A. Robbins, A.A. Sosunov, and P.A. Schwartzkroin. 2003. Mouse strain differences in kainic acid sensitivity, seizure behavior, mortality, and hippocampal pathology. *Neuroscience.* 122:551–561.

Meighan, S.E., P.C. Meighan, P. Choudhury, C.J. Davis, M.L. Olson, P.A. Zornes, J.W. Wright, and J.W. Harding. 2006. Effects of extracellular matrix-degrading proteases matrix metalloproteinases 3 and 9 on spatial learning and synaptic plasticity. *J. Neurochem.* 96:1227–1241.

Michaluk, P., and L. Kaczmarek. 2007. Matrix metalloproteinase-9 in glutamate-dependent adult brain function and dysfunction. *Cell Death Differ.* 14:1255–1258.

Monea, S., B.A. Jordan, S. Srivastava, S. DeSouza, and E.B. Ziff. 2006. Membrane localization of membrane type 5 matrix metalloproteinase by

AMPA receptor binding protein and cleavage of cadherins. *J. Neurosci.* 26:2300–2312.

Morimoto, K., M. Fahnestock, and R.J. Racine. 2004. Kindling and status epilepticus models of epilepsy: rewiring the brain. *Prog. Neurobiol.* 73:1–60.

Nagy, V., O. Bozdagi, A. Matynia, M. Balcerzyk, P. Okulski, J. Dzwonek, R.M. Costa, A.J. Silva, L. Kaczmarek, and G.W. Huntley. 2006. Matrix metalloproteinase-9 is required for hippocampal late-phase long-term potentiation and memory. *J. Neurosci.* 26:1923–1934.

Nedivi, E., D. Hevroni, D. Naot, D. Israeli, and Y. Citri. 1993. Numerous candidate plasticity-related genes revealed by differential cDNA cloning. *Nature.* 363:718–722.

Oh, L.Y., P.H. Larsen, C.A. Krekoski, D.R. Edwards, F. Donovan, Z. Werb, and V.W. Yong. 1999. Matrix metalloproteinase-9/gelatinase B is required for process outgrowth by oligodendrocytes. *J. Neurosci.* 19:8464–8475.

Okulski, P., T. Jay, J. Jaworski, K. Duniec, J. Dzwonek, F. Konopacki, G. Wilczynski, A. Sanchez-Capelo, J. Millet, and L. Kaczmarek. 2007. TIMP-1 abolishes MMP-9-dependent long-lasting long-term potentiation in the prefrontal cortex. *Biol. Psychiatry.* 62:359–362.

Oray, S., A. Majewska, and M. Sur. 2004. Dendritic spine dynamics are regulated by monocular deprivation and extracellular matrix degradation. *Neuron.* 44:1021–1030.

Pang, P.T., H.K. Teng, E. Zaitsev, N.T. Woo, K. Sakata, S. Zhen, K.K. Teng, W.H. Yung, B.L. Hempstead, and B. Lu. 2004. Cleavage of proBDNF by tPA/plasmin is essential for long-term hippocampal plasticity. *Science.* 306:487–491.

Pitkanen, A., and T.P. Sutula. 2002. Is epilepsy a progressive disorder? Prospects for new therapeutic approaches in temporal-lobe epilepsy. *Lancet Neurol.* 1:173–181.

Proper, E.A., A.B. Oestreicher, G.H. Jansen, C.W. Veelen, P.C. van Rijen, W.H. Gispen, and P.N. de Graan. 2000. Immunohistochemical characterization of mossy fibre sprouting in the hippocampus of patients with pharmaco-resistant temporal lobe epilepsy. *Brain.* 123:19–30.

Reeves, T.M., M.L. Prins, J. Zhu, J.T. Povlishock, and L.L. Phillips. 2003. Matrix metalloproteinase inhibition alters functional and structural correlates of deafferentation-induced sprouting in the dentate gyrus. *J. Neurosci.* 23:10182–10189.

Represa, A., I. Jorquera, G. Le Gal La Salle, and Y. Ben-Ari. 1993. Epilepsy induced collateral sprouting of hippocampal mossy fibers: does it induce the development of ectopic synapses with granule cell dendrites? *Hippocampus.* 3:257–268.

Shiosaka, S. 2004. Serine proteases regulating synaptic plasticity. *Anat. Sci. Int.* 79:137–144.

Shubayev, V.I., and R.R. Myers. 2004. Matrix metalloproteinase-9 promotes nerve growth factor-induced neurite elongation but not new sprout formation in vitro. *J. Neurosci. Res.* 77:229–239.

Singec, I., R. Knoth, M. Ditter, C.E. Hagemeyer, H. Rosenbrock, M. Frotscher, and B. Volk. 2002. Synaptic vesicle protein synaptoporin is differently expressed by subpopulations of mouse hippocampal neurons. *J. Comp. Neurol.* 452:139–153.

Sperk, G. 1994. Kainic acid seizures in the rat. *Prog. Neurobiol.* 42:1–32.

Sternlicht, M.D., and Z. Werb. 2001. How matrix metalloproteinases regulate cell behavior. *Annu. Rev. Cell Dev. Biol.* 17:463–516.

Sutula, T., P. Zhang, M. Lynch, U. Sayin, G. Golarai, and R. Rod. 1998. Synaptic and axonal remodeling of mossy fibers in the hilus and supragranular region of the dentate gyrus in kainate-treated rats. *J. Comp. Neurol.* 390:578–594.

Suzuki, F., Y. Makiura, D. Guilhem, J.C. Sorensen, and B. Onteniente. 1997. Correlated axonal sprouting and dendritic spine formation during kainate-induced neuronal morphogenesis in the dentate gyrus of adult mice. *Exp. Neurol.* 145:203–213.

Szklarczyk, A., J. Lapinska, M. Rylski, R.D. McKay, and L. Kaczmarek. 2002. Matrix metalloproteinase-9 undergoes expression and activation during dendritic remodeling in adult hippocampus. *J. Neurosci.* 22:920–930.

Takumi, Y., V. Ramirez-Leon, P. Laake, E. Rinvik, and O.P. Ottersen. 1999. Different modes of expression of AMPA and NMDA receptors in hippocampal synapses. *Nat. Neurosci.* 2:618–624.

Tian, L., M. Stefanidakis, L. Ning, P. Van Lint, H. Nyman-Huttunen, C. Libert, S. Itohara, M. Mishina, H. Rauvala, and C.G. Gahmberg. 2007. Activation of NMDA receptors promotes dendritic spine development through MMP-mediated ICAM-5 cleavage. *J. Cell Biol.* 178:687–700.

Toni, N., P.A. Buchs, I. Nikonenko, P. Povilaitite, L. Parisi, and D. Muller. 2001. Remodeling of synaptic membranes after induction of long-term potentiation. *J. Neurosci.* 21:6245–6251.

Vu, T.H., J.M. Shipley, G. Bergers, J.E. Berger, J.A. Helms, D. Hanahan, S.D. Shapiro, R.M. Senior, and Z. Werb. 1998. MMP-9/gelatinase B is a key regulator of growth plate angiogenesis and apoptosis of hypertrophic chondrocytes. *Cell.* 93:411–422.

Wu, Y.P., C.J. Siao, W. Lu, T.C. Sung, M.A. Frohman, P. Milev, T.H. Bugge, J.L. Degen, J.M. Levine, R.U. Margolis, and S.E. Tsirka. 2000. The tissue plasminogen activator (tPA)/plasmin extracellular proteolytic system regulates seizure-induced hippocampal mossy fiber outgrowth through a proteoglycan substrate. *J. Cell Biol.* 148:1295–1304.

Yong, V.W. 2005. Metalloproteinases: mediators of pathology and regeneration in the CNS. *Nat. Rev. Neurosci.* 6:931–944.